LARGE GAS BUBBLES UNDER THE ANODES OF ALUMINUM ELECTROLYSIS CELLS

Alexandre Caboussat[1,2,4], László Kiss[3], Jacques Rappaz[4], Klára Vékony[3], Alexandre Perron[5], Steeve Renaudier[6], Olivier Martin[6]

[1]Ycoor Systems SA, Technopôle 10, 3960 Sierre, Switzerland
[2]University of Houston, Department of Mathematics, 4800 Calhoun Rd, Houston, TX 77204-3008, USA
[3]Département des sciences appliquées, Université du Québec à Chicoutimi, 555 Boulevard de l'Université, Chicoutimi, Canada G7H 2B1
[4]Chaire d'Analyse et Simulation Numériques, École Polytechnique Fédérale de Lausanne, 1015 Lausanne, Switzerland
[5]Rio Tinto Alcan, CRDA, 1955 Boulevard Mellon CP 1250 Jonquière, Canada
[6]Rio Tinto Alcan, LRF, BP 114, 73303 Saint-Jean-de-Maurienne Cedex, France

Keywords: aluminum electrolysis, PIV, numerical simulations, two-phase flow, large bubbles, Fortin bubble.

Abstract

The gas bubble laden layer under the anodes during the electrolysis of alumina plays an important role in the hydrodynamics and the voltage balance of the reduction cells. Under certain geometrical and operational conditions, very large gas pockets, in the order of hundred cubic centimeters can be formed. The particular shape of these large gas bubbles was first described by Fortin et al in 1984 [1]. In the present paper the results of a combined experimental and numerical approach are described. In the experiments, the shape and the kinematics of the Fortin bubbles were analyzed by videography and Particle Image Velocimetry (PIV). A finite element method (FEM) combined with a Volume of Fluid (VOF) method was used to reproduce the experimentally observed phenomena, with particular attention to the reduction of the numerical diffusion of the liquid-gas interfaces. The morphology of the large bubbles and their movement including the velocity field around them are described.

Introduction

The gas bubbles generated during the electrochemical reduction of aluminum occupy a part of the horizontal inter-electrode space. Being electrical insulators, these bubbles induce a parasite voltage drop and cause an increase of the energy consumption of the cell. The electrical resistance of the bubble-laden layer under the anode is influenced by the quantity of the gas (volume fraction, covering factor) and by the morphology of the bubble layer. The electrical resistance of the molten electrolyte follows the fluctuations provoked by the random events of bubble nucleation, coalescence and escape of the bubbles [2]. In the past decade, significant efforts were invested into the clarification of the mechanisms of bubble-induced overvoltage by several researchers (see a review in [3]).

The electrical resistance of the bubble layer is considered by most of the researchers as an equivalent resistance of a heterogeneous medium with the electrolyte as the continuous conducting phase. The classical approach is that of Maxwell, who gave the first expression to calculate the equivalent (sometimes called "apparent" or "bulk") conductivity for a conducting medium with sparsely distributed spherical, identical isolating voids [4,5]. Later, Bruggemann developed a formula for spheres of non-uniform diameters [6], but still for voids that are sufficiently far from each other compared to their diameters.

Physical modeling in laboratory, as well as numerical simulations show [1,7] that the real situation is far from the case of sparsely distributed spherical bubbles. Under the anodes with dimensions common in today's industry, the growth by coalescence produces very big bubbles with shapes that are not similar to the usual

notion of bubbles. The present paper deals with these so-called *Fortin bubbles*, studying their morphology and behavior both by experiments and by mathematical modeling and numerical simulations.

Experiments

Experimental setup

Large bubbles under the anodes were studied using low-temperature hydrodynamic models. Two different setups were constructed. In the first, the large bubbles were produced by coalescence under a porous plate that represents the anode bottom. Such an arrangement produces a bubble layer and bubble driven flow similar to that in real reduction pots, but it does not permit studying the hydrodynamics of the large bubbles separately from other effects as the continuous interactions with smaller bubbles, the fluctuating velocity of the bubble layer, etc. For this reason, a second experimental rig was developed that makes possible to study of the morphology and kinematics of the Fortin bubbles in its pure form. In the experiments presented here, water and air were used as fluids. The bubbles were produced one-by-one under the lower end of the inclined solid surface (Figure 1), by using the so-called inverted cup technique that permits to produce bubbles precisely with the desired volume of the gas.
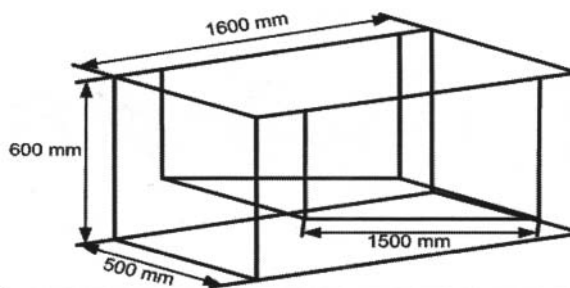

Figure 1. Schema of the experimental setup

In order to follow the movement and shape evolution of the bubbles, they were recorded by high-speed video cameras. Images were taken from the side, using a rail mounted, moving camera, as well as from the bottom by the help of an inclined mirror under the water pool.

Image processing was extensively used for extracting quantitative information about the shape and velocity of the bubbles. The necessary algorithms and codes were developed by using MATLAB©. Different edge-detecting algorithms were tested to

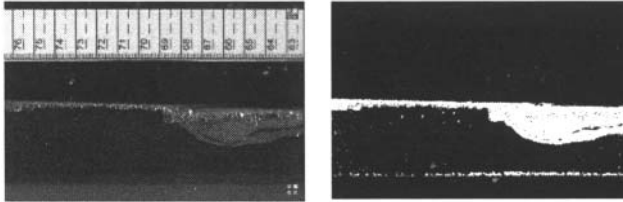follow the contour of the Fortin bubbles. An illustrative example is shown below in Figure 2.

Figure 2. Image before and after using the threshold filter

Particle image velocimetry

Besides the analysis of the morphology and movement of the large bubbles, the velocity field in the liquid phase was also studied quantitatively by using particle image velocimetry (PIV).
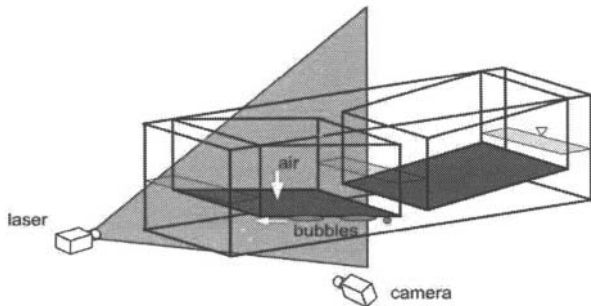

Figure 3. Using PIV in a two-anode hydrodynamic model.

The measurement is illustrated in Figure 3 for a two-anode arrangement, but the principle is the same for the single bubble setup shown in Figure 1. The flow is seeded with small tracer particles whose settling velocity is negligible. A pulsed laser sheet illuminates the selected planar section of the fluid volume and a camera records consecutive images of the tracer particles. Two of these images are used to determine the velocity vectors in the illuminated plane.

Figure 4. Instantaneous velocity field around a Fortin bubble

Both instantaneous and time-averaged velocity fields were determined. The example in Figure 4 shows an instantaneous velocity pattern around a large Fortin-bubble whose contour is marked by the dashed line in the image.
Figure 5 was obtained by averaging instantaneous velocity distributions obtained during the passage of several bubbles. In the image, the magnitude of the velocity distribution is shown by superposing a colored contour plot of the magnitude of the velocities on top of the vector plot.
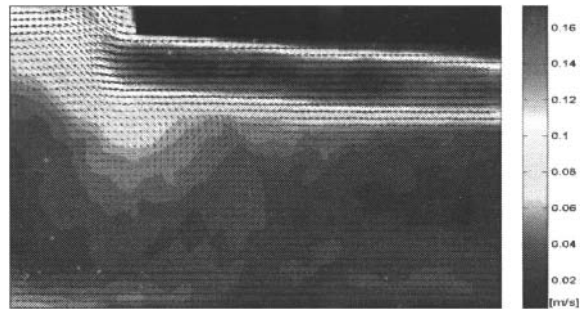

Figure 5. Mean bath velocity close to the side channel at 2° of angle of inclination

Morphology of bubbles

Since the first description of the morphology of large bubbles by Fortin et al. [1], its shape is characterized mostly by the side view. It is particular that around the leading edge of the moving bubble a so-called "head" is formed, which has a penetration depth at least twice that of the static or slowly moving bubbles. This is a typically dynamic phenomenon – stationary bubbles never have this head, independently of their volumes. Another interesting feature of the shape of Fortin bubbles is that in the plane of the solid surface (see right view of Figure 6) the leading edge takes a nearly perfect circular form. In three dimensions, the surface of the Fortin bubble is complex, the typical contour, as it is shown in Figure 4, is a longitudinal, central section. When filming laterally, this central section is mostly hidden, depending on the method of illumination (see the left image in Figure 6).
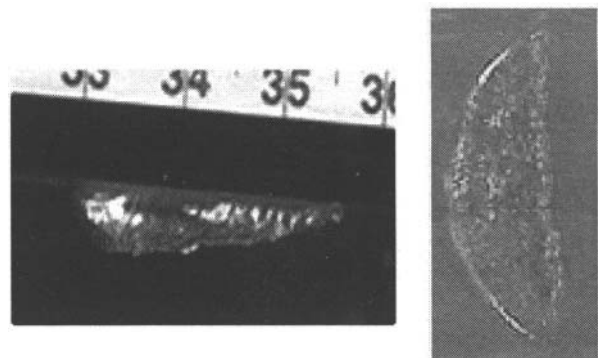

Figure 6. Side and bottom views of a 150 ml Fortin bubble, 4° inclination

The head of the Fortin bubble follows the curvature of the leading edge in the plane of the solid surface; its shape reminds of a croissant cut in half. Analyzing many Fortin bubbles, the shape was approximated by a schematic geometry as shown in Figure 7. The cross section of the head is described by a parabola that follows the circular arc of the leading edge.
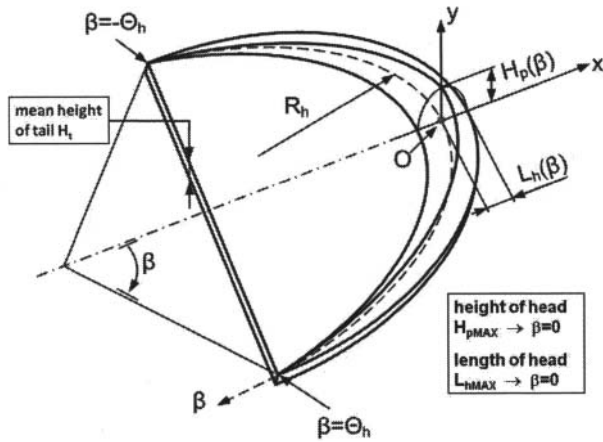
Figure 7. Analytical approximation of the geometry of a Fortin bubble

Using the notation of the schema, the volume of the gas in the bubble can be calculated according the formula below

$$V_{bubble} = A_{contac\_shape} \cdot H_t + \frac{32}{21} \cdot H_{p_{max}} \cdot L_{h_{max}} \cdot R_h \cdot \frac{\pi \cdot \Theta_h^\circ}{180^\circ}$$

where $\quad H_p(\beta) = H_h(\beta) - H_t$

Modeling and Numerical Simulation

A two-phase flow model and an Eulerian algorithm are proposed for the numerical simulation of the hydrodynamics of large bubbles under an inclined plane. This numerical model is inspired from [8,9]. Unlike in [10,11], where the complete magneto-hydrodynamic problem is considered, this model focuses on the *hydrodynamics of a single large bubble* only and is used to describe the morphology of these bubbles.

Physical model

Let Λ be the cavity (aluminum cell, more precisely the electrolytic bath) in which the fluid is confined, and let $T > 0$ be the final time of simulation. For any given time t, let Ω_t be the domain occupied by the liquid and let Γ_t be the free surface defined by $\partial\Omega_t \backslash \partial\Lambda$. The notations are shown in Figure 8 for a large bubble initially located under an inclined plane, under the effect of gravity forces.
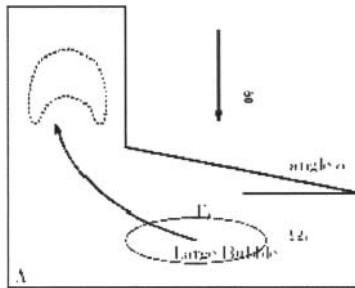

Figure 8. Large bubble of gas under an inclined plane, subject to gravity forces.

Compressible gas bubbles in the incompressible fluid in modeling represent the bubbles nucleating during aluminum reduction. A

volume-of-fluid approach is used to track the liquid domain and the free surface. Let φ be the characteristic function of the liquid domain (φ equals one if liquid is present, zero if it is not). In order to describe the kinematics of the free surface, φ satisfies the following transport equation in the cell Λ:

$$\frac{\partial\varphi}{\partial t} + \mathbf{v} \cdot \nabla\varphi = 0,$$

where $\mathbf{v}$ denotes the velocity of the two-phase fluid in Λ. The incompressible Navier-Stokes equations are assumed to hold in the liquid domain Ω_t (varying in time), which implies that the velocity $\mathbf{v}$ and the pressure p of the liquid satisfy, in Ω_t, the equations of conservation of mass and momentum:

$$\rho\frac{\partial\mathbf{v}}{\partial t} + \rho(\mathbf{v} \cdot \nabla)\mathbf{v} - 2\nabla \cdot (\mu\mathbf{D}(\mathbf{v})) + \nabla p = \mathbf{f},$$

$$\nabla \cdot \mathbf{v} = 0,$$

where ρ and μ are the density and viscosity of the fluid respectively, $\mathbf{D}(\mathbf{v})=0.5(\nabla\mathbf{v} + \nabla\mathbf{v}^T)$ denotes the symmetric tensor of deformations, and $\mathbf{f}$ represents the external forces (typically $\mathbf{f}$ is the sum of gravity forces and electromagnetic Lorentz forces). Here we consider only $\mathbf{f} = \rho\mathbf{g}$, where $\mathbf{g}$ is the gravitational field as represented in Figure 8. The bubbles of gas are composed of an ideal, isothermal gas: the velocity in the gas is disregarded and we assume that the product of the gas pressure P times the bubble volume is constant in each bubble of gas. The connected components of the gas domain (bubbles) have to be tracked at each time step. The force applied on the free interface Γ_t between the liquid and the gas is given by

$$-p\mathbf{n} + 2\mu\mathbf{D}(\mathbf{v})\mathbf{n} = -P\mathbf{n} + \sigma\kappa\mathbf{n},$$

where σ is the (constant) surface tension coefficient between the liquid and gas, κ is the curvature of the interface, and $\mathbf{n}$ is the normal vector to the interface, oriented outside the liquid domain. Appropriate essential boundary conditions on the boundary of the cell $\partial\Lambda$ and initial conditions on the bubble position and velocity are added to close the mathematical model. Note that the numerical method does not include any representation for the mechanism of the nucleation of bubbles.

Numerical model

We advocate a numerical method based on a *splitting algorithm* for the time discretization, and a *two-grid method* for the space discretization. The splitting algorithm allows decoupling the physical phenomena and solving each of them sequentially at each time step. It is illustrated in Figure 9. At each time step, two advection problems are solved first, leading to a prediction of the new velocity, together with the new approximation of the characteristic function of the liquid domain. They consist in solving

$$\frac{\partial\varphi}{\partial t} + \mathbf{v} \cdot \nabla\varphi = 0,$$

$$\frac{\partial\mathbf{v}}{\partial t} + \mathbf{v} \cdot \nabla\mathbf{v} = 0.$$

This allows determining the new liquid domain, the new gas domain and the new liquid-gas interface. Then the bubbles of gas are tracked with an original *numbering algorithm* (see [8,9]) and a

583

constant pressure is computed in each bubble by applying the ideal gas law. The surface tension effects are taken into account by computing an approximation of the curvature of the interface together with the external normal vector, by using the so-called *continuum surface force* model. Finally, a Stokes problem is solved, in the liquid domain only, to compute the final velocity in the liquid and its pressure. The corresponding equations are:

$$\rho\frac{\partial \mathbf{v}}{\partial t} - 2\nabla \cdot (\mu \mathbf{D}(\mathbf{v})) + \nabla p = \rho \mathbf{g},$$

$$\nabla \cdot \mathbf{v} = 0,$$

The pressure in the gas and the surface tension effects are applied on the free surface as an external force, and appropriate boundary conditions (e.g. slip or no-slip boundary conditions) are added.
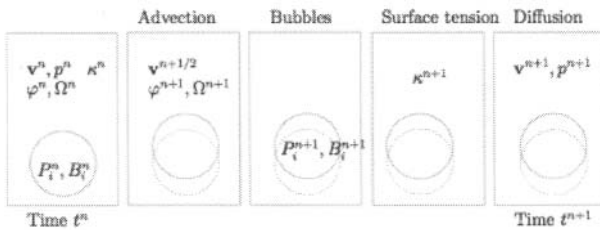
Figure 9. The splitting algorithm decouples the physical phenomena: From left to right: transport equations, tracking of bubbles and computation of gas pressure, computation of surface tension effects, and diffusion equations (Stokes problem).

A two-grid method is used for the spatial discretization, as illustrated in Figure 10: a regular grid of small cells is used to solve the transport equations (left), while the solution of the Stokes problem is performed on an unstructured finite element mesh composed of tetrahedrons (right). The solutions are interpolated at each time step between the two grids with projections operators. In order to reduce numerical diffusion effects of the free interface motion and to balance accuracy and computational cost, the structured grid is typically five to ten times finer than the finite element mesh.

A method of forward characteristics allows to obtain piecewise constant approximations of a prediction of the velocity and of the volume fraction of liquid on the structured grid of small cells. It is coupled with geometric reconstruction algorithms of the liquid-gas interface to reduce numerical diffusion. Adaptive subdivision techniques for the finite element mesh have been proposed in [12] to further reduce the numerical diffusion.

Stabilized (Galerkin least-squares-style) piecewise linear finite elements, based on piecewise affine finite element approximations of the velocity and pressure, are used for the approximation of the solution of the generalized Stokes problem. The tracking of the bubbles and the computation of their pressure has been described in [9]; it is achieved by solely solving Poisson problems with piecewise linear finite element approximations. The approximation of the surface tension effects has been detailed in [8]; it relies on variational arguments for the computation of the mean curvature of the interface. The complete algorithm is an order one algorithm in space and time.
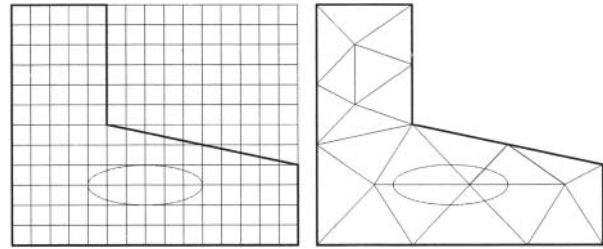
Figure 10. Two grids method in the two-dimensional case: structured grid of small square cells (left) and unstructured finite element mesh of triangles (right).

Numerical setup and morphology indicators for Fortin bubbles

Numerical simulations are undertaken in order to compare the experimental results in [13,14,15,16] with those obtained by mathematical and numerical modeling. Such comparisons are achieved thanks to a set of indicators describing the shape and morphology of the Fortin bubble under an inclined anode. These indicators are namely the *length* of the Fortin bubble L, the *maximal height* of the Fortin head H_h, the *maximal length* of the Fortin head L_h, the *mean height* of the bubble H_t and the *width* W of the bubble in a plane parallel to the surface of the anode. The notation is detailed in Figure 7. The mean height is measured at the middle of the Fortin bubble.

Several configurations for the Fortin bubble and the inclined anode have been considered in [16]. We consider here inclination angles of 1, 2, 4 and 8 degrees, and bubbles of different sizes. Experiments in [16] have been undertaken with bubbles of volumes 50, 150 and 250 ml. The geometry and dimensions of the computational domain of the corresponding numerical simulations is a subset of the one illustrated in Figure 1. The *anode-cathode distance* (ACD) is set to approximately 4 cm. The density, viscosity and surface tension coefficients are those of the water and water-air interface and respectively given by $\rho=1000$ kg/m^3, $\mu=0.001$ kg/(ms) and $\sigma=0.0728$ N/m. The gravity forces are $\mathbf{g} = -9.81\ \mathbf{e}_z$ m/s^2 (oriented vertically).

Numerical Results

An illustration of the Fortin bubble obtained by numerical simulation is given in Figure 11. A single bubble of initial volume 250 ml evolves under an inclined plane with an angle of 8 degrees. It illustrates a three-dimensional contour of the bubble (A), a cut in the middle vertical section, showing the typical Fortin head (B), a cut along an inclined plane parallel to the anode surface (C), and a representation of the mesh that is purposely finer in the layer under the anode where the bubble evolves. One can observe that small residual parts of the large bubble are left behind during the process, similarly to the behavior found experimentally.
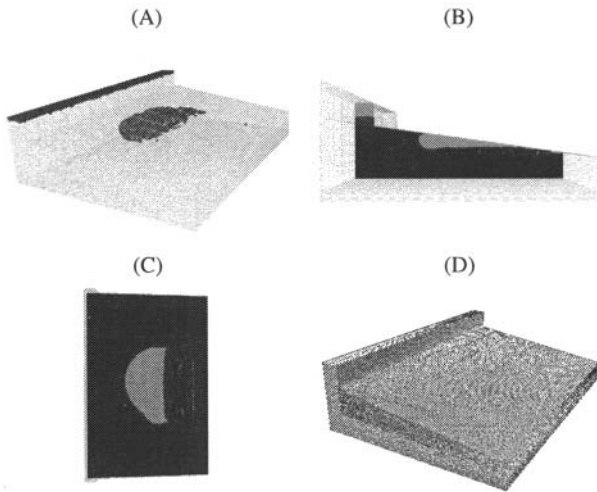
584

(A)   (B)

(C)   (D)

Figure 11. Illustration of a Fortin bubble of volume 250 ml under an inclined plane of 8 degrees. (A) contour of the bubble; (B) cut in the middle vertical plane; (C) cut in the plane parallel to the inclined anode; (D) illustration of the 3D mesh used for the numerical simulation.

Comparisons and discussion

A comparison of the morphology of the Fortin bubble between the numerical results and the experimental ones is based on the indicator variables L, H_h, L_h, H_t and W. We consider first a bubble with initial volume 250 ml and various inclination angles for the anode.

We compare the length L and width W of the bubble. Results are illustrated in Figure 12. Experimental results are taken from [16]. Numerical results are obtained by applying either slip or no-slip boundary conditions on the surface of the anode. When enforcing slip boundary conditions on the anode, the bubble can slide on its surface; when enforcing no-slip boundary conditions, the bubble sticks to the surface.
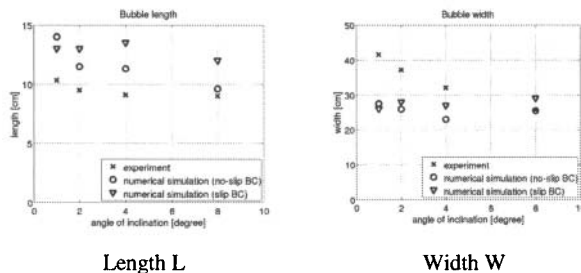

Length L   Width W

Figure 12. Comparison of bubble's length and width between experiments and simulations for a bubble's volume of 250 [ml] and various inclination angles. Influence of the boundary conditions applied on the anode.

Although not quantified here, the measurement errors are relatively large for both the experiments and the simulations. We can observe that the length of the simulated bubble is slightly overestimated, while its width is underestimated, indicating that the numerical solution may not be completely stationary. Note also that the influence of the type of boundary conditions is of the same order as the error on the measurements.

Figure 13 illustrates the other morphological indicators, namely H_h, L_h and H_t for no-slip boundary conditions only. Conclusions are similar, as the match between simulations and experimental data is consistent. Sources of errors include measurement issues, but also discrepancies in the exact volumes of bubbles (as the volume of the simulated bubble is slightly larger than 250 ml), differences of ACD distances and water height, and questions related to the influence of the meshes.
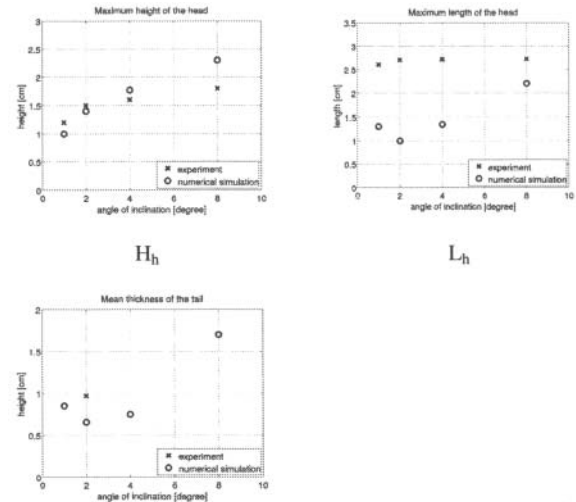

H_h L_h

Figure 13. Comparison of the maximal height of the Fortin head H_h, the maximal length of the Fortin head L_h, and the mean height of the bubble H_t for a bubble's volume of 250 ml and various inclination angles.

In a second step, we consider an inclined angle of 8 degrees and various volumes for the bubble, ranging from 140 ml to 300 ml. Figure 14 shows comparison of the results for the quantities L, H_h, L_h and W. Simulations and experiments exhibit the same trends for the morphology of the Fortin bubble.

These numerical results also express the physical instability of the Fortin bubble, which is similar to the one of a rising buoyancy bubble (see for instance [8,17] and references therein).

Length L   Width W
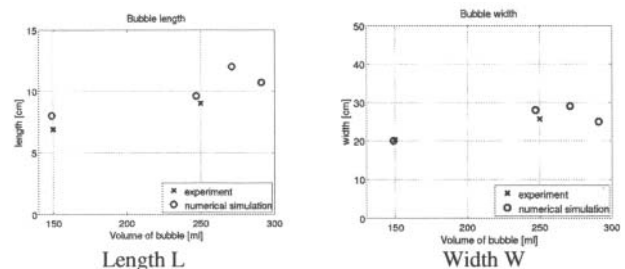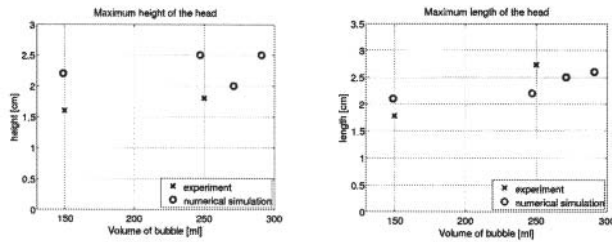
Height of the head H_h Length of the head L_h

Figure 14. Comparison of morphology indicators between experiments and simulations for an inclined plane with an angle of 8 degrees and various bubble volumes.

Finally a comparison between the numerical results and the velocity data obtained with particle image velocimetry (PIV) techniques is briefly sketched. The quantitative interest is in the *terminal velocity of the bubble* (in the quasi-stationary state of the Fortin bubble). For a Fortin bubble with volume 250 ml and an inclination angle of 8 degrees, the terminal velocity obtained by PIV and reported in [16] is given by 32 cm/s. In the numerical simulations, the bubble velocity is computed by considering the displacement of the bubble in a given time interval. Simulations lead to a terminal velocity in the range 28-35 cm/s for volumes between 250 and 290 ml. Instantaneous velocities in a cut in the middle of the bubble are illustrated in Figure 15. Note that the mathematical model does not compute a velocity inside the bubble, and therefore the velocity in the gas phase is set to zero. These preliminary results allow us to conclude to the consistency of the velocity values between experimental and numerical results, and will be detailed in future works.
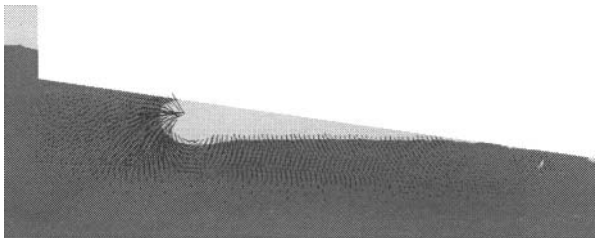

Figure 15. Instantaneous velocity field around the Fortin bubble obtained by numerical simulation.

Conclusions

Large bubbles under an inclined anode have been studied both experimentally and numerically. These bubbles are formed during the aluminum electrolysis. From the experimental point of view, videography and particle image velocimetry (PIV) allow to describe the morphology of Fortin bubbles and terminal velocities. From the numerical viewpoint, a volume-of-fluid method and finite element approximations have been used to reproduce experiments. Comparisons of the results have exhibited similar morphologies of bubbles, comparable quantified results and similar trends in the morphology of bubbles, when varying the inclination angle of the anode or the volume of the bubble.

Acknowledgments

References

[1] S. Fortin, M. Gerhardt, and J. A. Gesing. Physical modeling of bubble behavior and gas release from aluminum reduction cell anodes. TMS Light Metals, pp. 721–741, 1984.

[2] M. V. Romerio, A. Lozinski and J. Rappaz. A new modeling for simulating bubble motions in a smelter. TMS Light Metals, pp. 547–555, 2005.

[3] M.A. Cooksey, M. P. Taylor and J.J.J. Chen, Resistance Due to Gas Bubbles in Aluminum Reduction Cells, Journal of Metals, pp. 51-57, 2008.

[4] A. Perron, L. I. Kiss, and S. Poncsàk. Mathematical model to evaluate the ohmic resistance caused by the presence of a large number of bubbles in Hall-Héroult cells. J. Applied Electrochemistry, 37, pp. 303–310, 2007.

[5] J.C. Maxwell, A Treatise on Electricity and Magnetism, 3rd ed. New York, Dover Pub., 1954.

[6] D. Bruggeman, Annalen der Physik, 24, pp. 636–664, 1935.

[7] S. Poncsák, L. Kiss, D. Toulouse, A. Perron and S. Perron, Size distribution of the bubbles in the Hall-Héroult cells, TMS Light Metals, pp. 457-462, 2006.

[8] A. Caboussat. A numerical method for the simulation of free surface flows with surface tension. Computers and Fluids, 35(10), pp. 1205–1216, 2006.

[9] A. Caboussat, M. Picasso and J. Rappaz. Numerical simulation of free surface incompressible liquid flows surrounded by compressible gas. J. Comput. Phys., 203(2), pp. 626–649, 2005.

[10] M. Flueck, T. Hofer, M. Picasso, J. Rappaz, and G. Steiner. Scientific computing for aluminum production. Int. J. Numer. Anal. and Modeling, 6(3), pp. 489–504, 2009.

[11] M. Flueck, A. Janka, C. Laurent, M. Picasso, J. Rappaz, and G. Steiner. Some mathematical and numerical aspects in aluminum production. J. Sci. Comp., 43(3), pp. 313–325, 2008.

[12] A. Caboussat, P. Clausen, and J. Rappaz. Numerical Simulation of Two-Phase Flow with Interface Tracking by Adaptive Eulerian Grid Subdivision, submitted to Int. J. Num. Meth. Fluids, 2010.

[13] A. Perron, L. I. Kiss, and S. Poncsák. An experimental investigation of the motion of single bubbles under a slightly inclined surface. Int. J. Multiphase Flow, 32, pp. 606–622, 2006.

[14] K. Vékony and L. I. Kiss. Morphology of two-phase layers with large bubbles. Metallurgical and Material Transactions B, pp. 1–12, 2010.

[15] K. Vékony and L. I. Kiss. Velocity measurements in a real size model of an aluminum electrolysis cell model using the PIV techniques, submitted to J. Applied Electrochemistry, 2010.

[16] K. Vékony. Large bubble moving under a solid surface. Ph.D. thesis, Université du Québec à Chicoutimi, 2009.

[17] S. Hysing, S. Turek, D. Kuzmin, N. Parolini, E. Burman, S. Ganesan, and L. Tobiska. Quantitative benchmark computations of two-dimensional bubble dynamics, Int. J. Num. Meth. Fluids, 60(11), pp. 1259—1288, 2009.